Synthesis lead of two-dimensional sheets by spark discharge in liquid nitrogen

Ahmad Hamdan, Hiba Kabbara, Cédric Noel, Jaafar Ghanbaja, Abdelkrim Redjaïmia, Thierry Belmonte

Synthesis of lead two-dimensional sheets by spark discharge in liquid nitrogen

Ahmad Hamdan[1,2], Hiba Kabbara[1], Cédric Noël[1,3], Jaafar Ghanbaja[1], Abdelkrim Redjaimia[1] and Thierry Belmonte[1,3,*]

[1]Université de Lorraine, Institut Jean Lamour, UMR CNRS 7198, NANCY, F-54042, France

[2]current address: Groupe de physique des plasmas, Université de Montréal, C.P. 6128, Succ. Centre-ville, Montréal, Québec, H3C 3J7, Canada

[3]CNRS, Institut Jean Lamour, UMR CNRS 7198, NANCY, F-54042, France

* corresponding author. Email: thierry.belmonte@univ-lorraine.fr

PACS numbers: 47.55.dr Interactions with surfaces; 52.80.Wq Discharge in liquids and solids ; 81.07. ± b Nanoscale materials and structures: fabrication and characterization

Keywords: discharge in liquids; plasma-surface interaction; nanoparticles; liquid nitrogen; lead

ABSTRACT

A simple method to synthesize hexagonal sheets of lead, which belong to the class of two-dimensional materials, is presented. These objects can be collected on a substrate located under two lead electrodes between which nanosecond-pulsed spark discharges in liquid nitrogen are ignited. The hexagonal sheets are single crystals produced by gas phase condensation. Once nitrogen is fully evaporated, they are oxidized in the air and turned into PbO_2. The oxidation process induces stress that may pleat the uppermost sheets or open cracks in the centre of the structure. The thickness of individual objects varies typically from 4 to 20 nm. If the number of discharges exceeds about 2000, two types of PbO_2 sticks start being observed: bundles made of nanosticks (5 μm in length and 50 nm of diameter) and isolated stick (20 μm in length and 500 nm in diameter) in addition to sheets. These new nanostructures are mainly due to the way lead electrodes are eroded by the discharge. At the beginning, the anisotropic erosion driven by the orientation of crystallographic planes of lead crystals produces octahedra and nanosticks, these latter growing longer and longer on electrode surfaces as discharges proceed. After about 2000 discharges, nanosticks are long enough to be easily broken, likely by mechanical stress, and fall onto the underlying substrate.

1. INTRODUCTION

Plasmas in liquids or in contact with liquids offer new challenges to understand and control interaction between plasmas and materials (Mariotti et al. 2010; Graham et al. 2011). Plasmas generated in liquids have attractive characteristics like high temperature, high pressure, high density of chemically active species, shock waves and intense radiation (Akiyama 2000). These environments open up new perspectives in two broad domains of research: materials (Mariotti et al. 2010) and medicine (Fridman et al. 2007, Li et al. 2009). Furthermore, discharges in liquids are known to present the highest production yields of nanomaterials by a physical method, which makes them particularly interesting for mass production at low-cost.

Because the electrodes can be considered as a reservoir of matter to synthesize nanoparticles (Schur et al. 2007), a large variety of materials can be processed by discharge in liquids. The use of various materials as anode and cathode can lead to the synthesis of metallic alloys or core-shell structures (Abdullaeva et al. 2012). The chemical and physical properties of the liquid play a critical role in this process. The liquid can be inert (nitrogen, helium…), reactive (water, alcohol…) or used as a source of matter (hydrocarbons, organosilicon…). For instance, discharges in hydrocarbons produce spontaneously carbon nanoparticles (Ahmed et al. 2009), while discharges in liquid nitrogen with carbon electrodes produce different carbon nanostructures, like nano-onions, nano-horns, nanowires, etc. (Sano and Ukita 2006). Electrical parameters also greatly affect the way electrodes are eroded and they modify the chemical processes in the plasma. At least, two main categories of electrical discharges can be defined: high current - low voltage (~100 A, 30 V) (Sano 2004) and high current - high voltage (~100 A, 10 kV) (Kuskova et al. 2007). Plasma ignition is only possible in the former category if electrodes are put in contact.

Concerning lead nanostructures, they have applications in several domains. They can be used for the development of sensors in nanotechnology. For example, metallopolymer films

containing lead nanoparticles exhibit sensor activity in the presence of ammonia (Bochenkov et al. 2002). Concerning lead oxide nanosheets, they might be useful as active materials of lead-acid batteries (Karami et al. 2008). Indeed, some studies showed that the morphology and size of the electrode components play an important role in the improvement of operating electrochemical activity of electrodes in batteries (Shi et al. 2008).

Deposition of lead thin films is of great scientific and technological importance in superconductivity. For example, let's mention the existence of a superconductor-insulator transition in lead thin films with disorder, where the apparition of superconductivity is defined by a critical sheet resistance (Trongin et al. 1970; Haviland et al. 1989). As this latter parameter is inversely proportional to the film thickness, the transition temperature rapidly decreases in ultrathin films (Eom et al. 2006).

Magnetic properties of lead are attractive for biomolecular studies in Nuclear Magnetic Resonance (NMR). Lead nanostructures can also be used as probes to study metal-ion binding sites in proteins. Thus, a large dispersion in chemical shift was observed for ^{207}Pb signals in proteins. This illustrates the remarkable sensitivity of this element to subtle differences in the chemical environment within proteins (Aramini et al. 1996).

In this work, we studied lead nanostructures grown by electrical discharges in liquid nitrogen between two lead electrodes submitted to high voltage and high current. Some experiments run in water instead of liquid nitrogen were made on purpose to clarify some aspects of the growth mechanisms. After a short description of the experimental setup, experimental results will be presented and the growth mechanism of nanostructures will be discussed.

2. EXPERIMENTAL SETUP

The experimental setup presented in figure 1a was used to study discharges in pin-to-pin configuration. Two wires made of lead were used as electrodes (source: GoodFellow, diameter: 0.5 mm; purity: 99.999 %). The distance between the two electrodes was set at 100

± 10 µm by using a micrometric screw. A high DC voltage power supply (Technix, SR15-R-1200 – 15 kV – 80 mA) feeds a high voltage solid-state switch (Behlke, HTS-301-03-GSM) that delivers, in a 50 nanosecond rise time, a current of about 30 A under a voltage of 10 kV for 300 ns typically (figure 1b). The operating frequency was 3 Hz (see reference (Ahmad et al. 2013) for more details). A Dewar vessel (volume: 400 cm^3) was filled with liquid nitrogen. On the bottom of the vessel, a substrate was left to collect the particles synthesized by successive discharges. Four kinds of substrates were used: silicon wafers, holey carbon grids, aluminium and 316 L stainless steel plates. The two last materials were polished mechanically (final stage 1 µm diamond paste) and ultrasonically cleaned in ethanol. After discharges processing, liquid nitrogen evaporated and the synthesized nanomaterials were exposed to air. They were readily available for characterization.

Scanning Electron Microscopy (SEM) – Quanta 600 FEG by FEI and XL 30 – was used for structural and chemical observations. The Quanta SEM is equipped with micro EDX (Energy-Dispersive X-ray) and it is used in mapping mode. XL 30 is equipped with a TLD detector (Through the Lens Detector) and it is used for high resolution imaging. Atomic force microscopy (AFM) analyses were performed using a SOLVER Nano device in semi-contact mode (free resonance at 100 kHz and force constant set at 2.0 N m^{-1}). A Philips CM200 device and a JEOL ARM200F cold FEG device were used for transmission electron microscopy (TEM) in order to study the morphology (with an atomic resolution), the crystallinity and the chemical composition of nano-objects.

During processing, the volume of liquid nitrogen is kept constant by compensating regularly losses due to evaporation. The growth mechanisms as well as the influence of the number of discharges on the synthesized nanostructures are thoroughly studied. Four cases are investigated: 100, 300, 1000 and 2000 discharges. The number of discharges is an important

parameter which is directly related to the etching of lead electrodes by the plasma and then, to the nature of the synthesized objects, as presented thereafter.

3. RESULTS AND DISCUSSION

3.1. Synthesized nano-objects

After evaporation of liquid nitrogen, the surface of the substrate can be covered by different types of nano-objects. By weighting the substrate after a set of discharges, we could estimate the average deposition rate per discharge is ~1.0 µg. Figure 2 shows large-view SEM images of the most commonly encountered objects at 1000 and 2000 discharges:

1- hexagonal or half hexagonal sheets (~5 µm in diameter and several nanometres in thickness) (figures 2a and 2c).

2- isolated sticks (~500 nm in diameter and ~20 µm in length) together with bundles of nanosticks (~50 nm in diameter and ~5 µm in length) (figures 2b, 2d and 2e),

These results are reproducible: the same type of objects being observed after the same number of discharges. More generally, reproducibility of experiments, after a given time of treatment, is satisfactory as far as the shape, the size distribution, the composition and the electrode mass loss are concerned. What is meant here by satisfactory is a possible variation of about 30% typically of the size distribution. Shape and composition are almost identical from one experiment to another. The electrode mass loss was found to vary by less than 5%.

These objects are also very stable in air, observation after more than one year giving identical results. Indeed, all nanostructures are made of lead only as long as they are in liquid nitrogen but they get oxidized as soon as they are put in the air. In this latter state, they are stable.

Other types of objects are also observed, but to a much lower extent.

3- hexagonal sheets can stack up, the uppermost sheets being pleated (figure 3a),

4- bundles of nanosticks as those mentioned earlier (2) can be put together in a slightly different way and adopt once in a while the shape of a butterfly (figure 3b),

5- nanowalls forming desert rose-like structures can be found (figure 3c), structures in which octahedral crystals are sometimes embedded (see supplemental material 1 and hereinafter),

6- nanoparticles (below 10 nm in diameter) are also present (figure 3d).

Stacking of nanosheets when the number of discharges is large enough is always observed. Using a moving substrate could limit this effect. However, no data is available yet on the cohesion of nanosheet stacks that might be either easily dispersed or kept as such when put in a solvent.

The number of discharges plays a crucial role on the nature of the synthesized nano-objects. To investigate the influence of this parameter, we proceeded as follows: four series with different numbers of discharges were run successively and the substrate was observed after each discharges series, *i.e.*, after 100, 300, 1000 and 2000 discharges.

Hexagonal sheets are observed on silicon wafers whatever the number of discharges but they are almost the only objects observed at small number of discharges (<1000 discharges). They are found together with few nanoparticles spread on the silicon surface. The thickness of one typical lead sheet was measured by AFM after 1000 discharges and it is ~8-10 nm in average (figure 4), but it may range between 4 and 20 nm. Hexagonal sheets occasionally have cracks in their centre and can even peel off (figure 5). Cracks are likely due to the mechanical stress in the sheets when they are heated up to room temperature during the evaporation of liquid nitrogen and simultaneously oxidized in ambient air. As edges are free, stress must develop in the centre of the structure.

After about 2000 discharges, sticks are observed on the collecting substrate. Some hexagonal sheets are also visible on the surface but they are partly covered by the sticks.

To sum up, we can say that hexagonal sheets are always synthesized but they cover almost exclusively the surface below 1000 discharges whereas nanosticks can only be seen beyond 2000 discharges. All other nanostructures are, by far, much less present.

For comparison, syntheses in deionized water were carried out, and the results are depicted in figure 6. Even though nanostructures are slightly less uniform and regularly spread, they are almost the same as those encountered in liquid nitrogen. Only some large micrometric beads are also found in this case. They are created by ejection of liquid droplets from the molten well formed by the spark. These micrometric objects attest of the violent interaction of the discharge interaction with a given electrode. Consequently, if the use of liquid nitrogen may be useful to form sheets, it is not mandatory.

3.2. Structure and chemical analysis

Hexagonal sheets are single crystals (figure 7). They belong to a new lead oxide phase. The identification of this phase has been achieved but was made extremely difficult by the lack of matter available, as no more than 1000 discharges can be run at a time, and by the two-dimensional structure of these objects that makes information along the *c*-axis very hard to extract. We could show anyway that lead oxide sheets crystallize in the Hexagonal *P-Bravais* lattice and belong to the $P\frac{6}{m}mm$ (or *P6mm*) space group, with the following lattice parameters: a = 0.9 nm and c = 1.75 nm.

EDX analyses were performed to show the chemical composition of the particles. As we can see in figure 8a, an hexagon is composed of lead dioxide (PbO_2), the quantification of the elements shows almost 66 at% of oxygen and 34 at% of Pb. In addition, STEM-EDX mapping were also carried out to show the elements distribution in one single hexagon (figure 8b), the Pb and O atoms are homogeneously distributed in in the hexagon.

We verified that nanosticks exhibit the same composition as hexagonal sheets (PbO_2). Concerning their crystallographic structure, it is likely the same as the sheets, as shown by

diffraction patterns, but since it was less investigated, no definitive proof can be brought at this stage.

3.3. Electrode erosion

The surface of the eroded electrodes was observed after 1000 and 2000 consecutive discharges in liquid nitrogen (figure 9). Electrodes are covered by bundles of nanosticks (figure 9a) of ~50 nm in diameter (figure 9b) which seem to emerge from the electrode bulk. These bundles grow at a given spot and in one bundle, nanosticks merging at the root. It is quite easy to understand how these nanostructures give rise to nanosticks, isolated sticks and butterfly-like structures. Either they break and fall individually into the liquid (figure 2d), or they agglomerate to form isolated sticks (figure 2e), or they get detached at their root and unfold to form the afore-mentioned butterfly-like structures (figure 3b). Similarly, octahedral crystals are also visible, as partly embedded in the lead electrode. The typical size of one octahedron is ~1-2 µm, like those observed in desert rose-like structures (supplemental material 1b).

On the other hand, when the number of discharges exceeds 2000, the surface of the electrodes is almost free of nanosticks (figure 9c) and octahedra get denser and larger (figure 9d). Obviously, the successive discharges etch the surface of the electrodes. Because of the polycrystalline structure of lead, etching of electrodes is anisotropic, the etching rate depending on crystals orientation. Octahedra correspond to the {111} dense planes of the *fcc* structure of lead. The key point here is the lack of 6-fold symmetry of these objects left on electrode surfaces. Then, there is no direct relationship between surface octahedra and hexagonal sheets.

The remarkable consequence of the presence of nanosticks and octahedra on the lead electrode surface is that the common view of a discharge at several thousand Kelvin that would evaporate everything is certainly wrong in the present situation. Let's recall here that

the melting point of lead is about 601 K only. We readily infer that the use of liquid nitrogen and/or very short discharges (~500 ns) must somehow favor a fast cooling and/or short heating of the material, which hinders an isotropic etching of the electrode. This has been already observed in our previous study (Ahmad et al. 2014) where the plasma emission in water was twice more intense than in liquid nitrogen.

For comparison, in the case of discharge in water, electrode erosion is characterized by the formation of craters at both electrodes (figures 10a and 10b). Classically, these craters are formed by the local melting of the electrode, which leads to a metal liquid well from which molten droplets can be ejected, forming the micrometric beads displayed in figure 6a. Interpenetrated nanowalls are clearly observed at the edge of the well (figure 10c). These nanostructures are similar to those found on desert rose-like structures (figures 3c and 6d). Next to the edge of the crater at the anode, temperatures are necessarily below the melting point of lead, enabling the growth of nanowalls perpendicularly to the surface. This shows the possibility of a moderate-temperature mediated process that drives the formation of nanowalls. In the case of discharges in liquid nitrogen, such areas made of nanowalls were observed on electrodes as well (figure 11), but in rarer case than in water. It is worth noting here that full and half hexagonal sheets are also present inside the crater as well as on the top of the protrusion. Thus, these sheets are deposited on the molten well on the electrode surface, exactly like they are on the substrate. We conclude that the growth of nanosheets is subsequent to the solidification of the metal well.

Consequently, nanowalls cannot be responsible for the presence of full (and likely of isolated half-) hexagonal sheets on the substrate. There are several reasons supporting this statement. First, nanowalls are in negligible amount in regards to sheets. Next, nanowalls and sheets, even though they exhibit similar shapes are geometrically different, the former being interpenetrated contrary to the latter. Finally, nanowalls growing on surfaces cannot lead to

full hexagons, but only to parts of hexagons. Thus, sheets and nanowalls are two different classes of objects obtained by two separated processes. Note that octahedra were not observed on the electrode surface after discharges in water, which means that the etching process depends on the liquid.

3.4. Growth mechanisms

We observe that nanosticks are synthesized at the electrode surfaces at the beginning of the process. As the discharge continues, their length increases and, after about 2000 discharges, they break and fall onto the substrate where they are collected. Their maximum length is then about 5 µm. We clearly observe in figure 5c for instance, that bundles of nanosticks are attached to the surface in a point which likely becomes the symmetry center of the butterfly-like structures observed on the silicon wafer, as already mentioned; the reason for such an arrangement is not clear yet.

Sheets, as explained before, have a different origin from nanowalls. Obviously, they do not grow on electrodes surface. Their 6-fold symmetry does not match the 4 fold-symmetry of octahedral, whose faces nevertheless exhibit this 6-fold symmetry. Because of the two-dimensional structure of these objects, we may conceive that they are formed by a surface process on the substrate used to collect them, *i.e.,* the silicon wafer here. In this case, the influence of the substrate on the growth mechanism should be essential. In addition to silicon wafers, the process was run with either aluminium, 316 L stainless steel or a holey carbon grid as substrates. After 300 discharges, we noticed the presence of sheets on all substrates. Those found on steel are ill-defined and sometimes hollow (figure 12). In the case of metallic substrates, a galvanic coupling very likely occurs between the lead sheets and the underlying metal, affecting the shape of the nanostructures. Otherwise, hexagonal sheets are identical

regardless of the substrate material. Then, the growth of these two-dimensional structures is not driven by surface processes.

Different methods on lead nanostructures growth have been reported in the literature (Yong et al. 2006a; Yong et al. 2006b, Yong et al. 2007, Shi et al. 2006, Lee et al. 2001; Jana et al. 2001). Zeng et *al.* (2012) synthesized hexagonal PbO sheets using gold nanoparticles. As suggested by the authors, growth can be driven by aggregation of different kinds of nanoparticles, each having a net dipole moment. They introduced a lead acetate solution into a mixture containing gold nanoparticles of 12 nm diameter. At room temperature and after 24 hours, PbO hexagonal sheet (size ~2.5 µm and thickness ~110 nm) appears in the solution. Zeng *et al.* (2012) suggested that the growth of sheet is obtained by aggregation of PbO nanoparticles were formed on the surface of gold nanoparticles. They proposed that the sheets formation is a result from an oriented attachment mechanism, in which the sheets form by aggregation of nanoparticles that each has a net dipole moment. Such a mechanism can probably not hold in our condition, only one type of nanoparticles being present. Besides, TEM analyses of lead oxide sheets in our case do not show any agglomerate sub-structure but only well-crystalline single-domain structures (figure 8).

On the other hand, Tang *et al.* (2006) studied the synthesis of CdTe sheets obtained by precipitating and ageing of CdTe nanoparticles in deionized water. They proposed two principal phenomena for the formation of sheets: i) an anisotropic electrostatic interactions between a dipole moment and a small positive charge and ii) directional hydrophobic attraction. This mechanism is also proposed for the formation of PbS ultrathin sheets (Schliehe et al. 2010). Compared to their results, the present sheets are characterized by a much narrower distribution of class of objects. In our case, and at short times, all hexagonal lead sheets have very similar shapes and sizes, which is not true for CdTe sheets (Tang *et al.* 2006). Such a growth mechanism is not expected to give regular structures. Nevertheless, we

performed syntheses by applying a negative voltage to the power electrode (−10 kV instead of +10 kV, the other electrode being grounded), and no significant modification was observed.

Contrary to sheets, nanowalls are expected to grow on surfaces. As explained previously, only certain spots, where moderate temperatures slightly below the melting point of lead prevail, are subjected to nanowall growth. Because of the similarity in shape between nanowalls and sheets, both growth modes have to be similar.

As a result of the foregoing, we propose the following growth mechanism. After breakdown in liquid nitrogen, a spark is formed between the electrodes. The main characteristics of such a discharge can be determined approximately by optical emission spectroscopy. Typically, the plasma has high temperature (5,000-10,000 K), high electron density (10^{16}-10^{17} cm^{-3}), high pressure (~5 MPa), and short lifetime (500 ns). The interaction of the spark discharge with electrodes etches the surface in an anisotropic manner, leaving octahedra, nanosticks and nanowalls at the electrode surface, and produces lead vapour whose condensation gives mainly sheets in the gas phase. Nanowalls are found on surface spots where the temperature is slightly lower than the melting point of lead. Then, the surface temperature of the electrodes remains low enough to enable differential erosion depending on the orientation of the lattice planes of lead. This temperature is probably also sufficiently low in the discharge to keep non-uniform growth rates of the lead sheets along the [111] axis of the *fcc* structure on the one hand and along the three other axes of the hexagons on the other hand. Indeed, if a hexagonal PbO_2 phase is observed in the end, it is because before oxidation by air, it was a [111]-oriented *fcc* Pb crystal (lead has no allotrope). So, we understand that the difficulty to etch the {111}-planes of the *fcc* lead structure, which enables the synthesis of octahedra at the electrode surface, makes the crystal growth slower in this direction, which gives naturally flat hexagons. Air oxidation turns the [111]-oriented *fcc* lead crystal into a [001]-oriented *hcp* lead oxide crystal. The location and period of time where the growth of the sheets holds in the gas

phase is unknown, the temperature gradient prevailing between the core of the discharge and the interface with liquid nitrogen being certainly huge anyway. Desert rose-like structures are simply grains covered by nanowalls which fall from the electrodes onto the substrate.

Finally, optimization of the process to produce weel-controlled lead oxide nanosheets requires several improvements. First, the change of the inter-electrode gap distance due to erosion by discharges should be compensated to keep a constant distance between electrodes. Second, the electrode tips should be changed before sticks break. This might be achieved by using as electrode a moving wire with a hairpin shape. Then, the inter-electrode gap distance would be kept constant in this case. Third, staking of lead hexagons should be avoided by using a moving substrate. Fourth, the size distribution of the nanosheets should be controlled. This issue could probably be solved by using lead electrodes with large grains (single crystals being likely to best material).

IV – CONCLUSION

In this work, we showed a new method to synthesize 2D-sheets of lead oxide. We showed that these objects grow by gas phase condensation and not by any surface process, either at the electrodes or at the substrate used to collect them. The use of ultrashort discharges together with the use of liquid nitrogen as dielectric favours the anisotropic growth of nanostructures. Furthermore, it gives rise to softer erosion when compared with deionized water. This paves the way to the controlled synthesis of non-spherical nanomaterials with this specific process.

Compliance with Ethical Standards:

Conflict of Interest: The authors declare that they have no conflict of interest.

REFERENCES

Abdullaeva Z, Omurzak E, Iwamoto C, Ganapathy S, Sulaimankulova S, Liliang C, Mashimo T (2012) Onion-like carbon-encapsulated Co, Ni, and Fe magnetic nanoparticles with low cytotoxicity synthesized by a pulsed plasma in a liquid. Carbon 50(5):1776–1785

Ahmed S, Aitani A, Rahman F, Al-Dawood A, Al-Muhaish F (2009) Decomposition of hydrocarbons to hydrogen and carbon. Appl Catal A: Gen 359(1):1–24

Akiyama H (2000) Streamer discharges in liquids and their applications. IEEE Trans Dielec Elec Insul 7(5):646–653

Aramini J, Yazawa T, Yuan T, Zhang M, Vogel H (1996) Lead-207 NMR: a novel probe for the study of calcium-binding proteins. J Biol Inorg Chem 1(1): 39–48

Bochenkov E, Stephan N, Brehmer L, Zagorskii V, Sergeev B (2002) Sensor activity of thin polymer films containing lead nanoparticles. Colloids Surf A Physicochem Eng Asp 198:911–915

Eom D, Qin S, Chou M-Y, Shih C (2006) Persistent Superconductivity in Ultrathin Pb Films: A Scanning Tunneling Spectroscopy Study. Phys Rev Lett 96(2):027005

Fridman G, Brooks A D, Balasubramanian M, Fridman A, Gutsol A, Vasilets V N, Ayan H, Friedman G (2007) Comparison of direct and indirect effects of non-thermal atmospheric-pressure plasma on bacteria. Plasma Process Polym 4(4):370–375

Graham W, Stalder K (2011) Plasmas in liquids and some of their applications in nanoscience. J Phys D: Appl Phys 44(17):174037

Hamdan A, Noel C, Ghanbaja J, Belmonte T (2014) Comparison of Aluminium Nanostructures Created by Discharges in Various Dielectric Liquids. Plasma Chem Plasma Proc 34(5):1101–1114

Hamdan A, Noel C, Kosior F, Henrion G, Belmonte T (2013) Impacts created on various materials by micro-discharges in heptane: Influence of the dissipated charge. J Appl Phys 113(4):043301

Haviland D, Liu Y, Goldman A (1989) Onset of superconductivity in the two-dimensional limit. Phys Rev Lett 62(18):2180–2183

Jana N R, Gearheart L, Murphy C J (2001) Evidence for seed-mediated nucleation in the chemical reduction of gold salts to gold nanoparticles. Chem Mater 13(7):2313–2322

Karami H, Karimi M A, Haghdar S, Sadeghi A, Mir-Ghasemi R, Mahdi-Khani S (2008). Synthesis of lead oxide nanoparticles by sonochemical method and its application as cathode and anode of lead-acid batteries. Mater. Chem. Phys. 108(2):337–344.

Kuskova N, Boguslavskii L, Smal'ko A, Zubenko A (2007) Obtaining nanocarbon using the electric-discharge treatment method of organic liquids. Surf Eng Appl Electrochem 43(4):269–275

Lee H J, Shon C H, Kim Y S, Kim S, Kim G C, Kong M G (2009) Degradation of adhesion molecules of G361 melanoma cells by a non-thermal atmospheric pressure microplasma. New J Phys 11(11):115026

Lee I, Han S, Choi H, Kim K (2001) Nanoparticle directed crystallization of calcium carbonate. Adv Mater 13(21):1617–1620

Mariotti D, Sankaran M (2010) Microplasmas for nanomaterials synthesis. J Phys D: Appl Phys 43(32):323001

Sano N (2004) Formation of multi-shelled carbon nanoparticles by arc discharge in liquid benzene. Mater Chem Phys 88(2):235–238

Sano N, Ukita S (2006) One-step synthesis of Pt-supported carbon nanohorns for fuel cell electrode by arc plasma in liquid nitrogen. Mater Chem Phys 99(2):447–450

Schliehe C, Juarez B, Pelletier M, Jander S, Greshnykh D, Nagel M (2010) Ultrathin PbS sheets by two-dimensional oriented attachment. Science 329(5991):550–553

Schur D, Dubovoy G, Zaginaichenko Y, Adejev M, Kotko V, Bogolepov A, , Savenko F, Zolotarenko D (2007) Production of carbon nanostructures by arc synthesis in the liquid phase. Carbon 45(6):1322–1329

Shi L, Xu Y, Li Q (2008) Controlled growth of lead oxide nanosheets, scrolled nanotubes, and nanorods. Cryst. Growth Design, 8(10):3521–3525.

Shi W, Zeng H, Sahoo Y, Ohulchanskyy T, Ding Y, Wang Z, Swihart M, Paras P (2006) A general approach to binary and ternary hybrid nanocrystals. Nano Lett 6(4):875–881

Tang Z, Zhang Z, Wang Y, Glotzer S, Kotov N (2006) Self-assembly of CdTe nanocrystals into free-floating sheets. Science 314(5797):274–278

Trongin M, Thompson R, Kammerer O, Crow J (1970) Destruction of superconductivity in disordered near-monolayer films. Phys Rev B 1(3):1078–1091

Yong K-T, Sahoo Y, Choudhury K, Swihart M, Minter J, Prasad P (2006a) Shape control of PbSe nanocrystals using noble metal seed particles. Nano Lett 6(4):709–714

Yong K-T, Sahoo Y, Choudhury K, Swihart M, Minter J, Prasad P (2006b) Control of the morphology and size of PbS nanowires using gold nanoparticles. Chem Mater 18(25):5965–5972

Yong K-T, Sahoo Y, Swihart M, Prasad P (2007) Shape control of CdS nanocrystals in one-pot synthesis. J Phys Chem C 111(6):2447–2458

Zeng S, Liang Y, Lu H, Wang L, Dinh X-Q, Yu X, Ho H-P, Hu X, Yong K-T (2012) Synthesis of symmetrical hexagonal-shape PbO sheets using gold nanoparticles. Mater Lett 67(1):74–77

FIGURE CAPTION

Figure 1: a) Experimental setup and b) electrical characteristics of one discharge in liquid nitrogen.

Figure 2: Large-view SEM images of a) hexagonal sheets synthesized after 1000 discharges and b) isolated sticks together with bundles of nanosticks. c) Detail of a hexagonal sheet. d) Detail of a bundle of nanosticks. e) Detail of an isolated stick.

Figure 3: Uncommon structures of lead obtained on silicon substrate by discharges in liquid nitrogen. a) Stacks of sheets, the uppermost being pleated. b) Nanostick bundles with butterfly shape. c) Desert rose-like structures. d) Nanoparticles. All these nanostructures are lead as long as they are in liquid nitrogen but get oxidized as soon as they are put in the air.

Figure 4: AFM topography image and height profiles along the two lines depicted in the AFM image. This example is representative of what is usually observed with other hexagonal sheets.

Figure 5: Unique hexagonal sheet presenting a crack in its centre. a) SEM image, b) TEM-BF image exhibiting better than the SEM image the distribution of the stress from the centre outwards.

Figure 6: Example of lead nanostructures observed after 1000 discharges in water. Same conditions as in liquid nitrogen. a) Lead beads mainly. b) Hexagonal sheets. c) Vertical half hexagonal sheets. d) Desert rose-like structures.

Figure 7: Overlapping of a TEM-BF micrograph of a lead oxide single crystal and the diffraction pattern of the corresponding object. Arrows show the directions that are perpendicular to the growth of the hexagon faces. The zone axis is [001].

Figure 8: EDX spectrum realized on a hexagonal particle and corresponding elemental composition. A micrograph of the lead oxide particle and its corresponding STEM-EDX oxygen map in blue and lead map in pink are depicted.

Figure 9: State of lead electrode (anode) after 1000 discharges in liquid nitrogen as observed by SEM at magnification a) ×20k and b) ×50k. State of lead electrode (anode) after 2000 discharges as observed by SEM at magnification c) ×12k and d) ×20k. Cathodes exhibit the same features as anodes.

Figure 10: State of lead electrode a) cathode and b) anode after 1000 discharges in deionized water. c) Magnification of the edge of the crater made in the anode showing the presence of nanowalls.

Figure 11: Nanowalls observed among nanosticks on the surface of a lead electrode eroded in liquid nitrogen.

Figure 12: Objects collected on a) aluminium, b) 316 L stainless steel and c) holey carbon grid.

Supplemental material 1: a) Desert rose-like structure without and b) with octahedral.

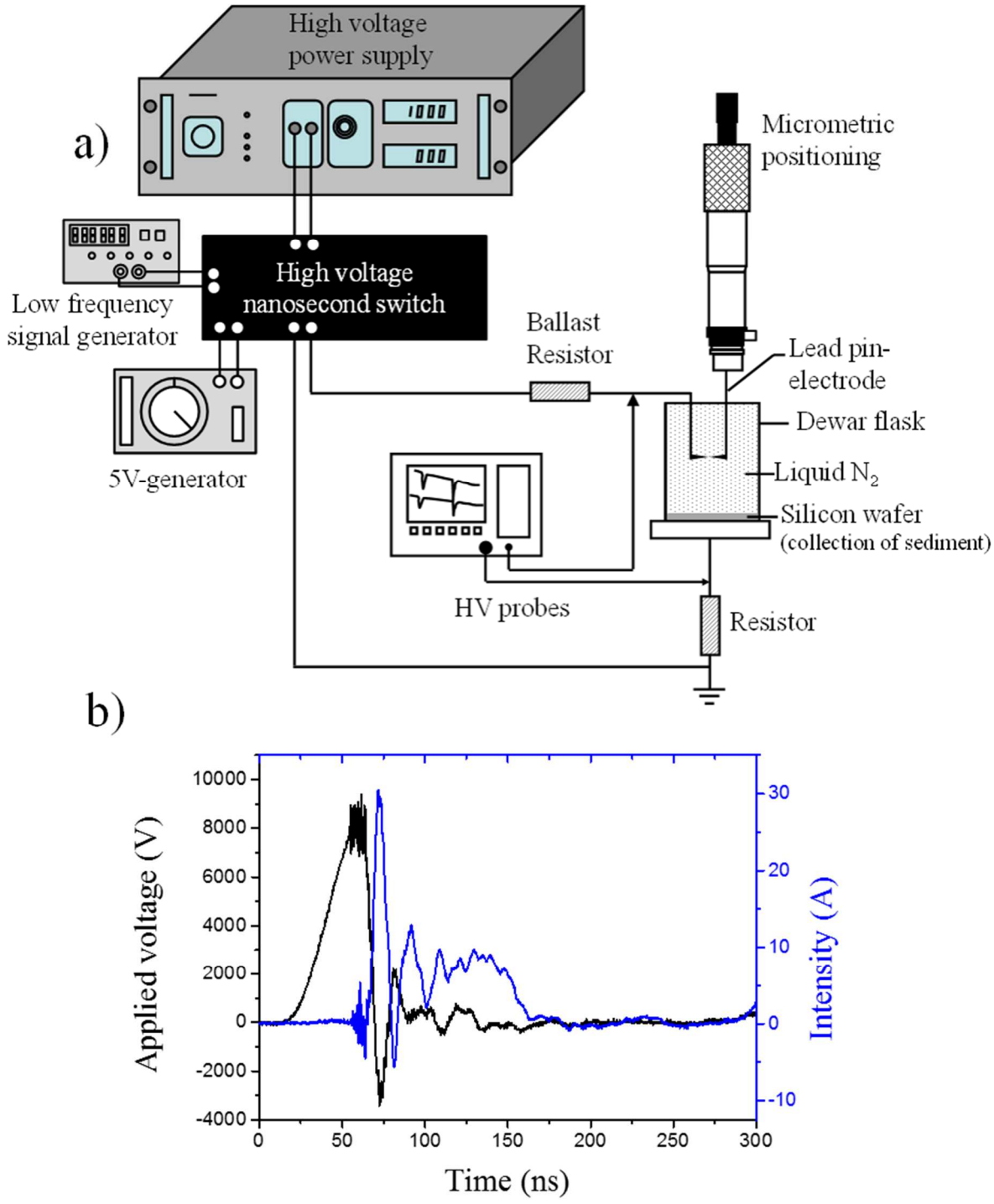

Figure 1 (black and white figure in print)

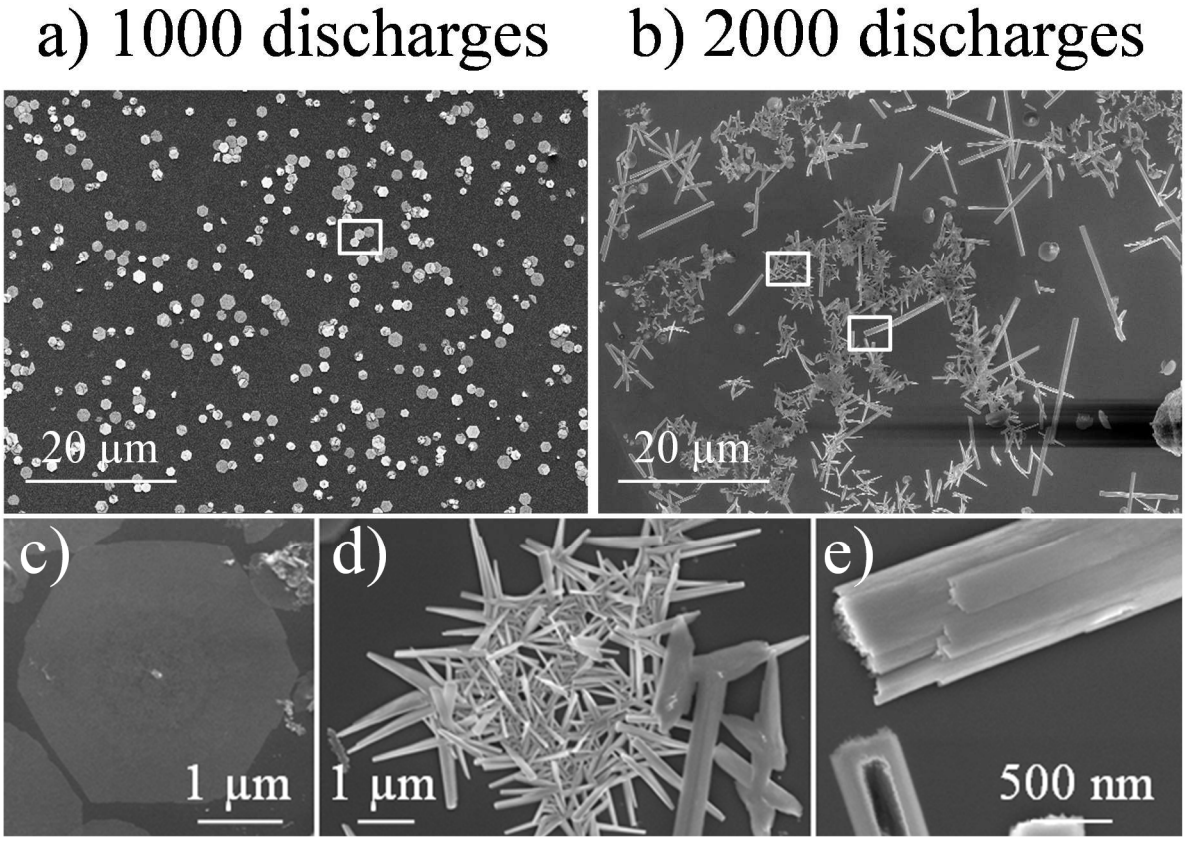

Figure 2 (black and white figure in print)

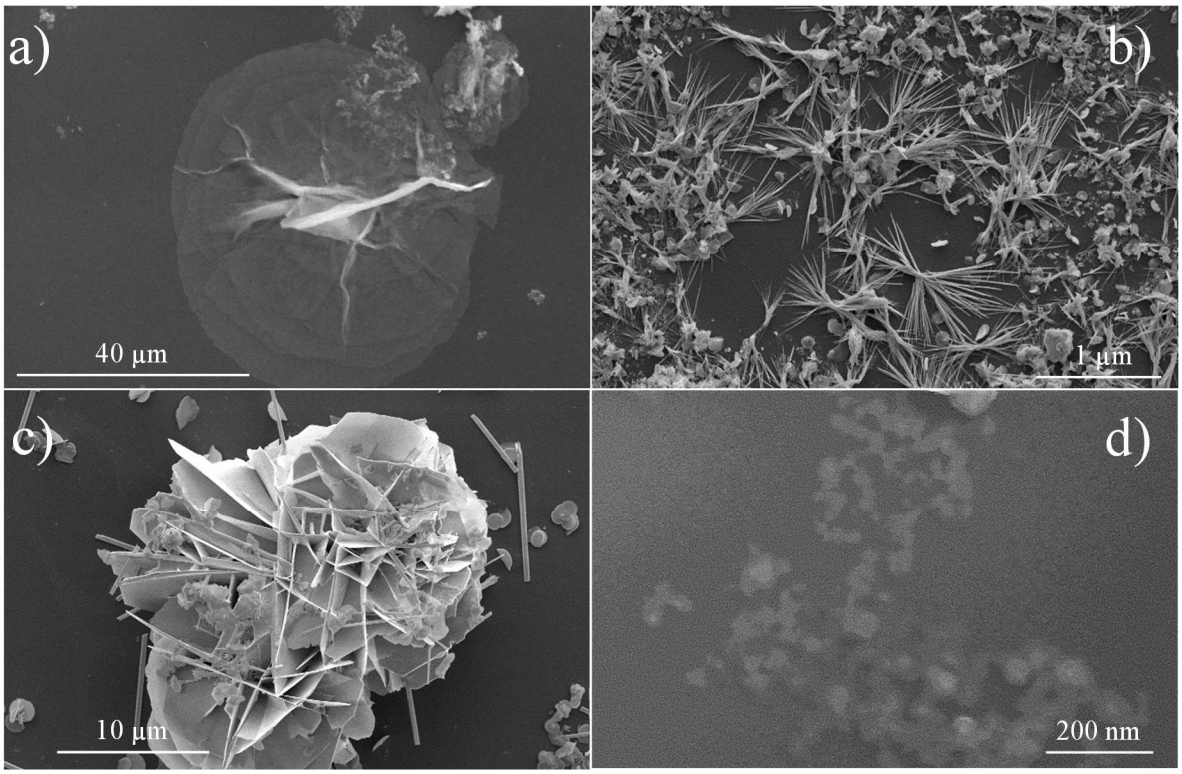

Figure 3 (black and white figure in print)

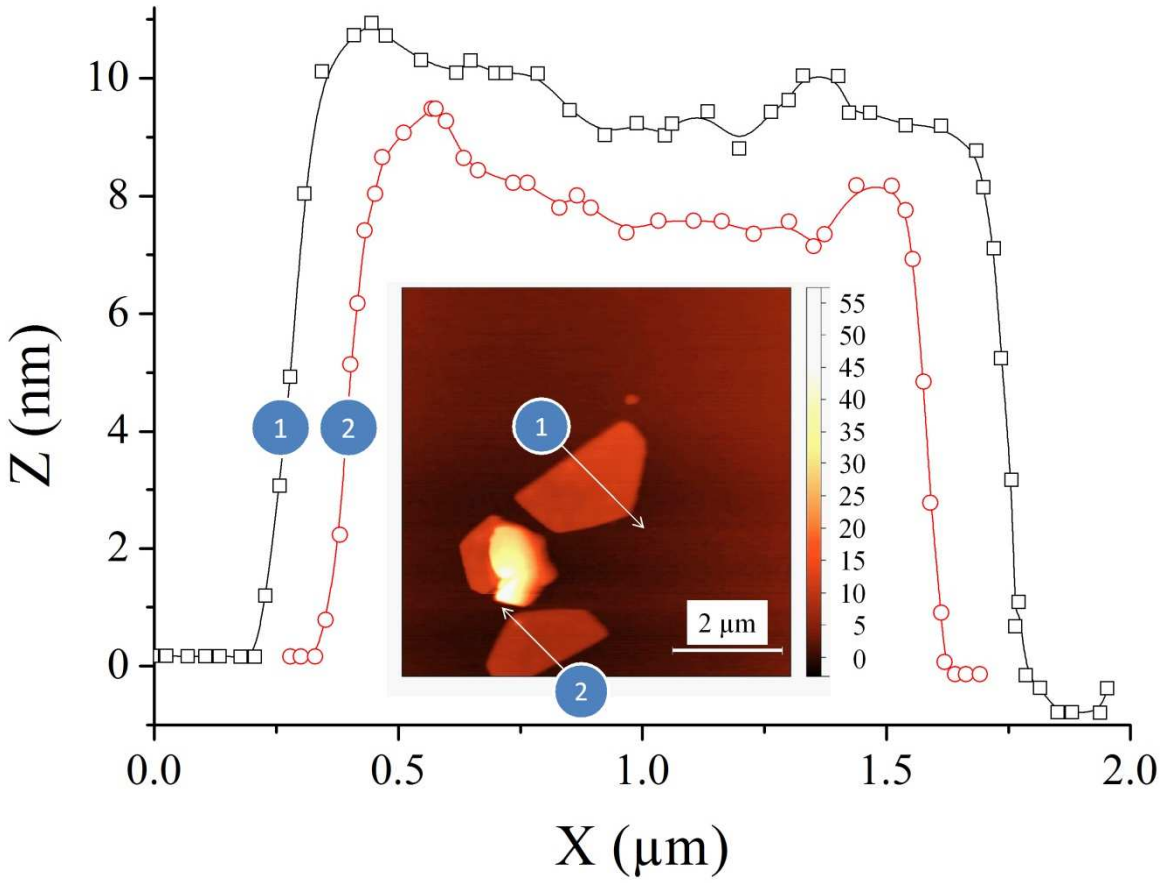

Figure 4 (black and white figure in print)

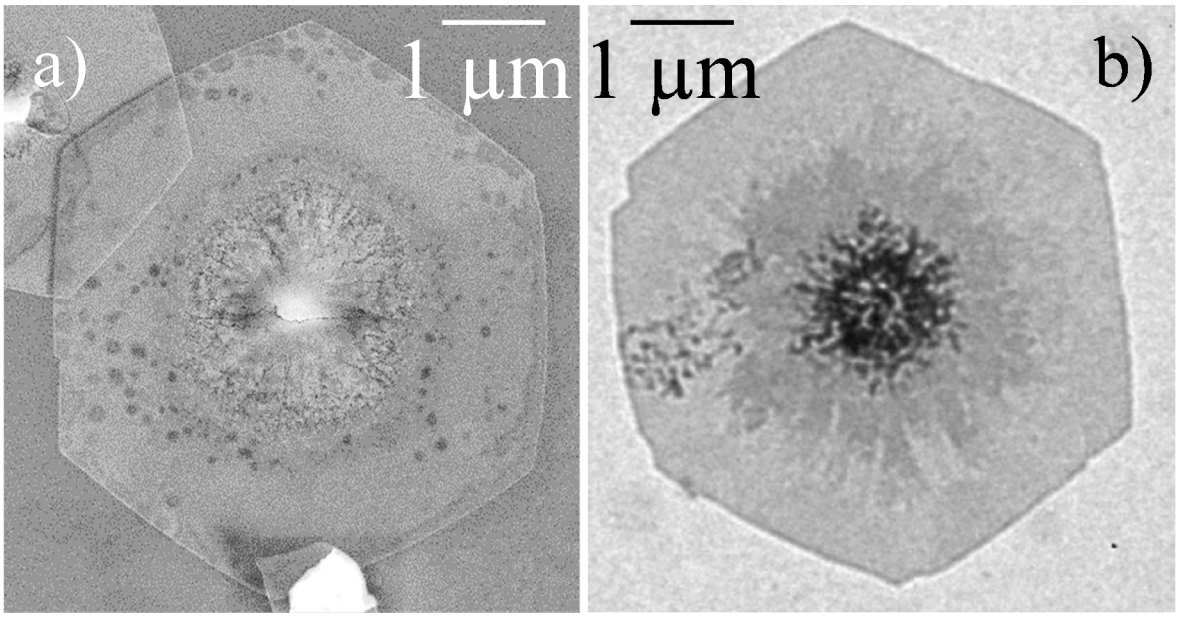

Figure 5 (black and white figure in print)

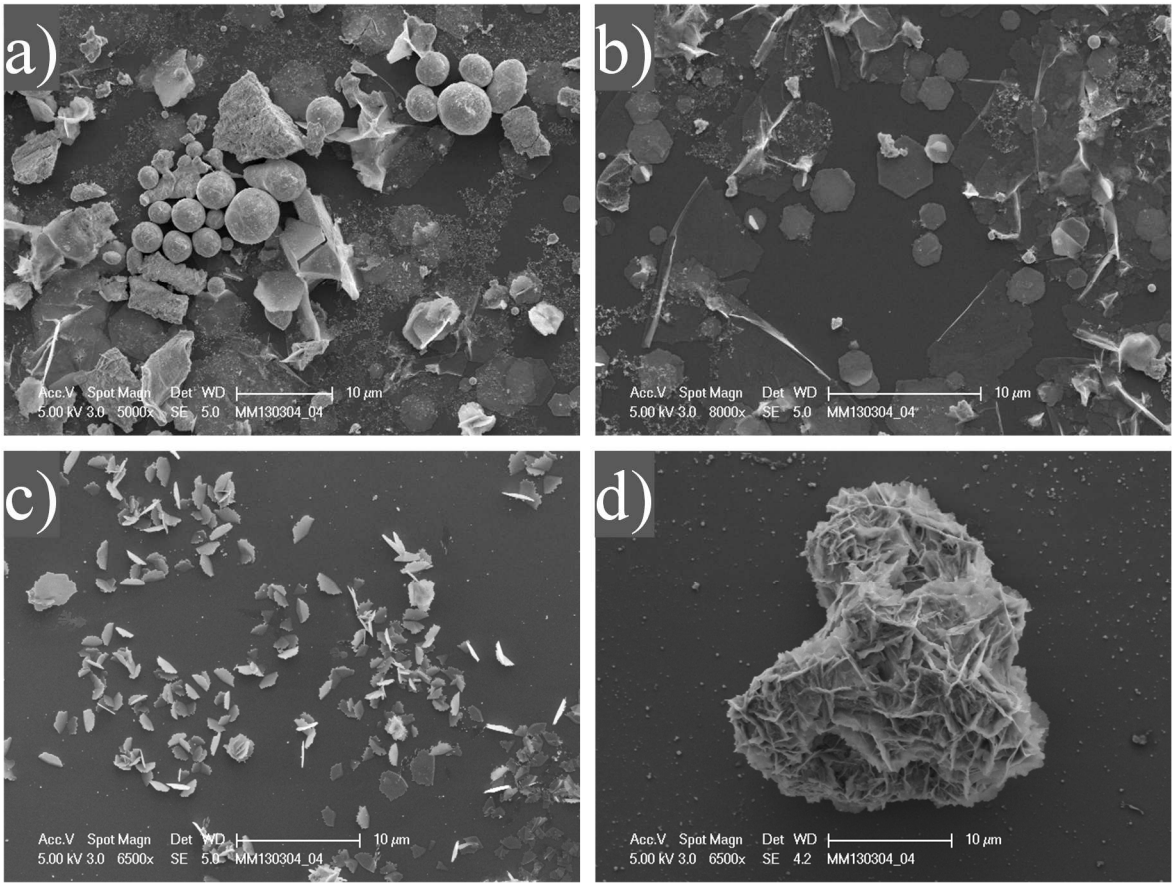

Figure 6 (black and white figure in print)

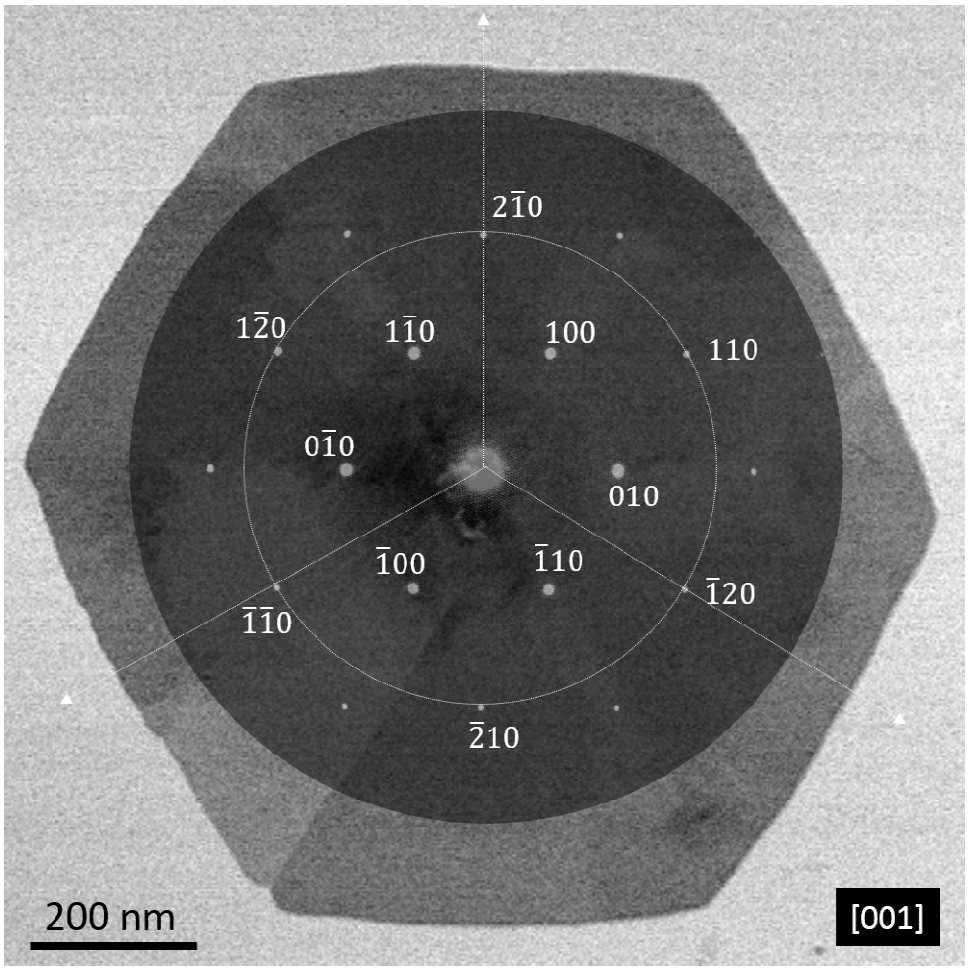

Figure 7 (black and white figure in print)

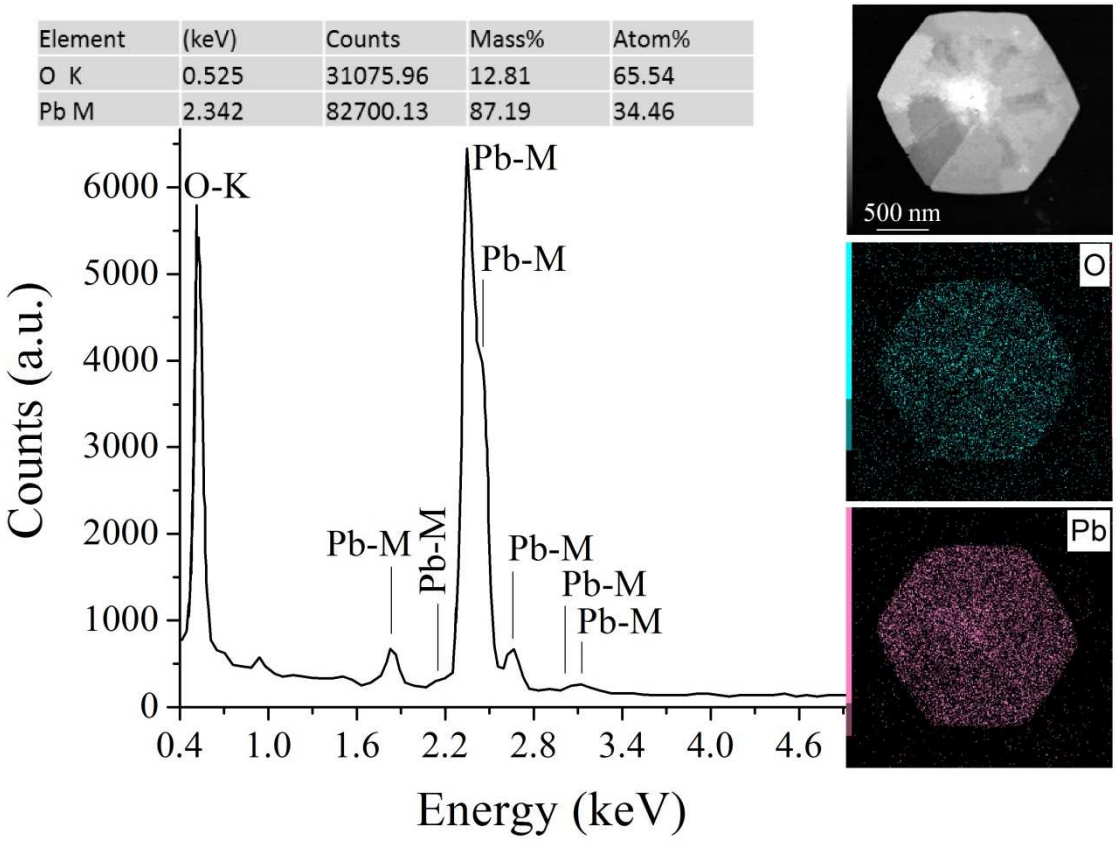

Figure 8 (black and white figure in print)

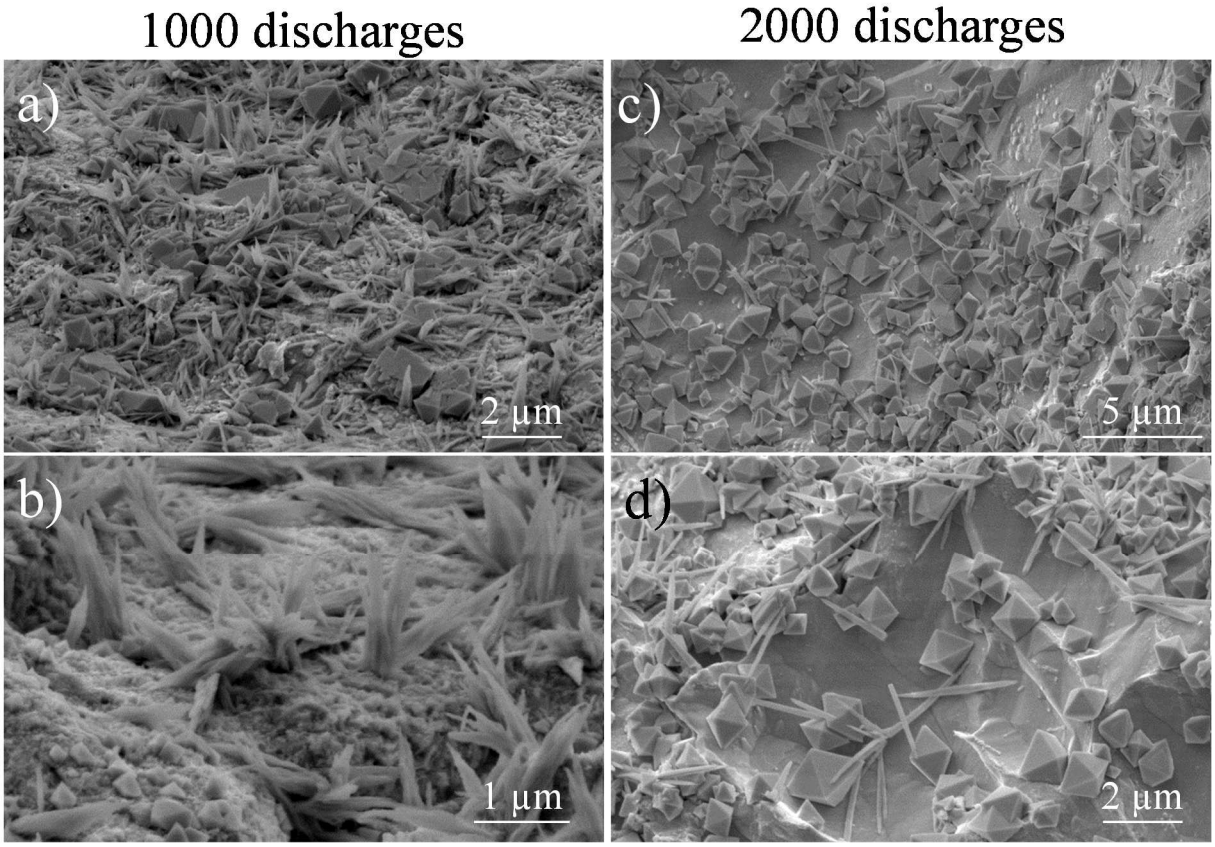

Figure 9 (black and white figure in print)

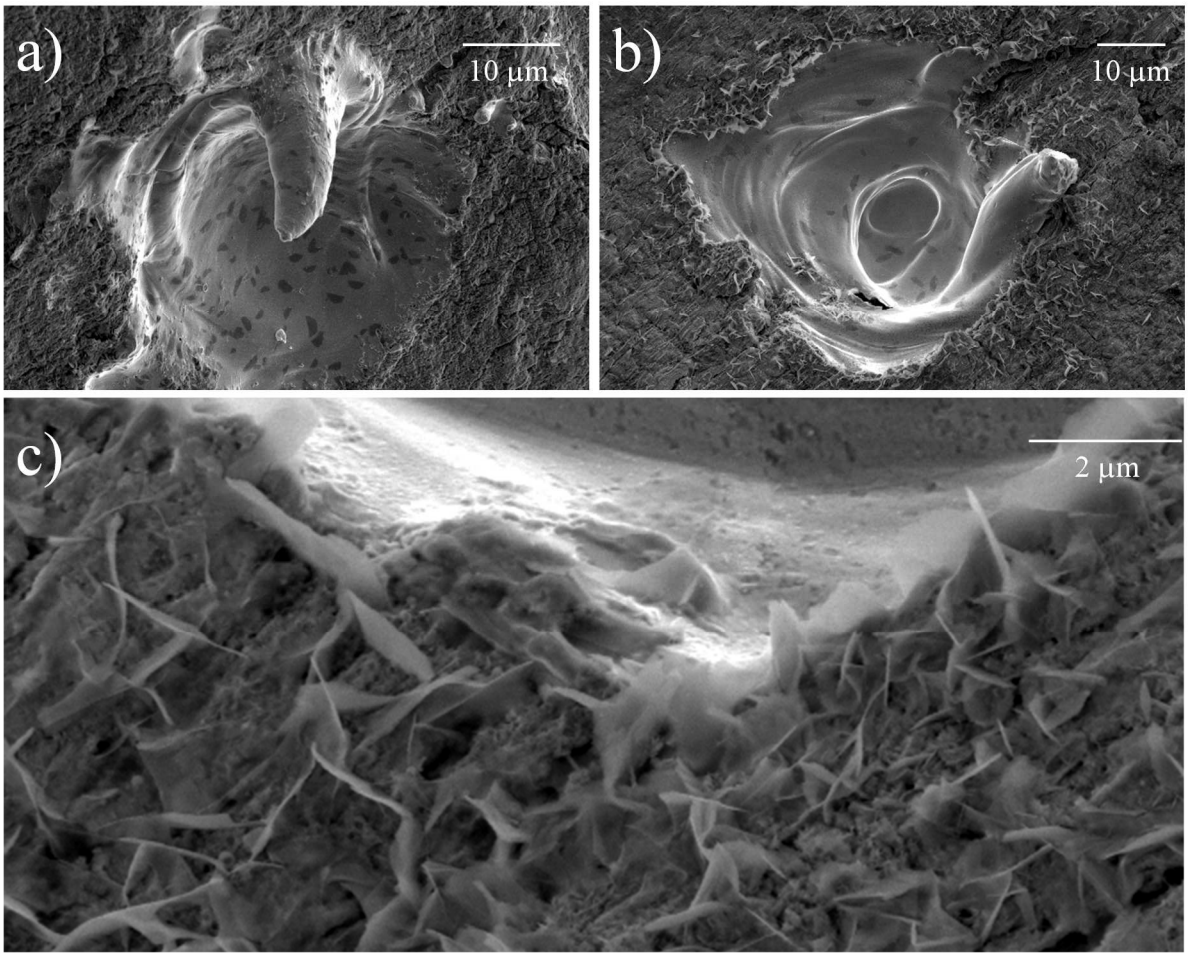

Figure 10 (black and white figure in print)

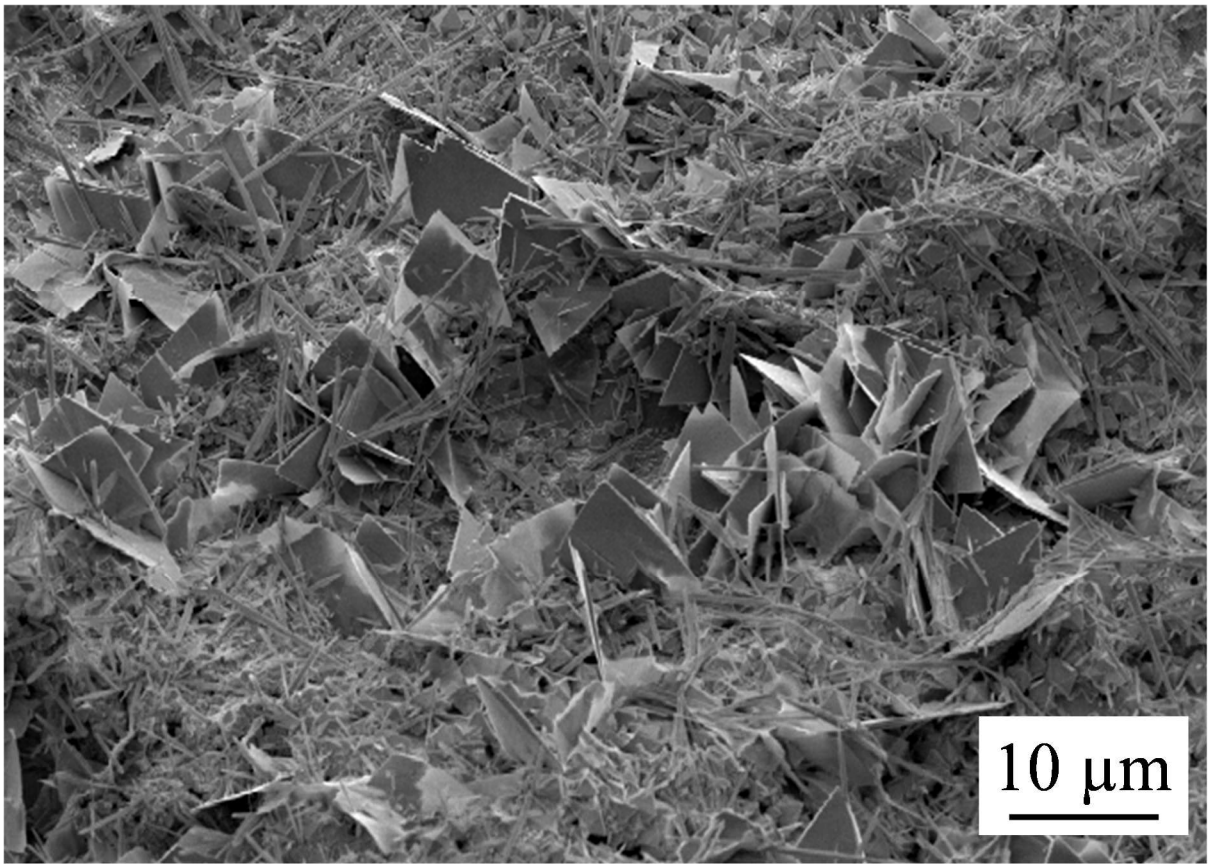

Figure 11 (black and white figure in print)

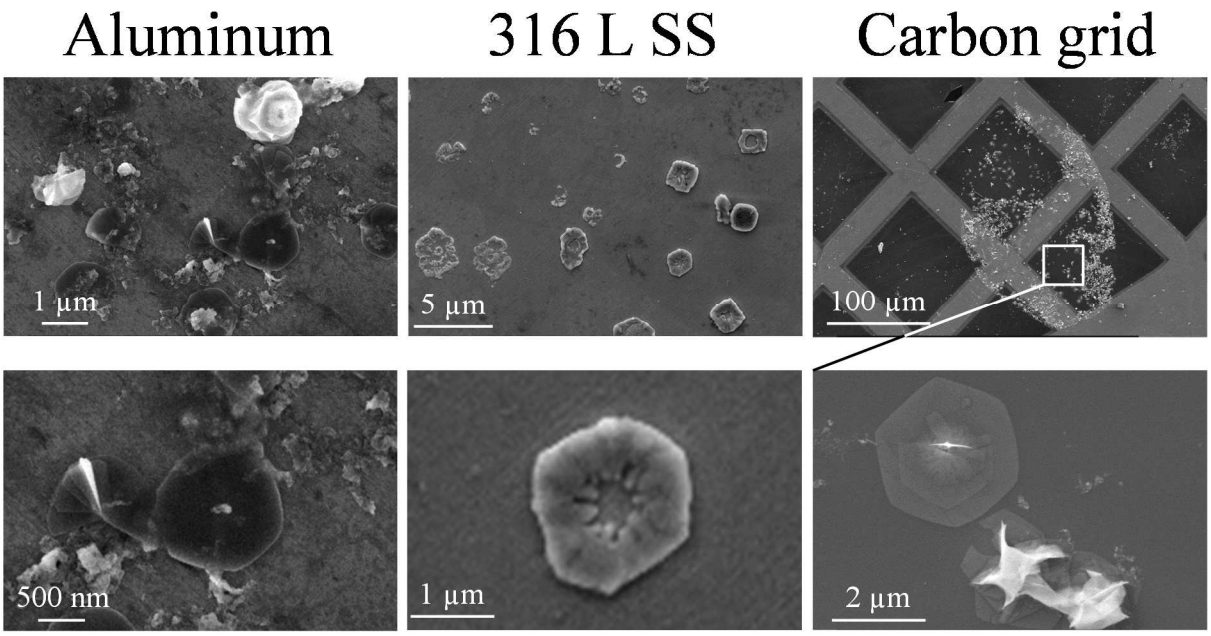

Figure 12 (black and white figure in print)

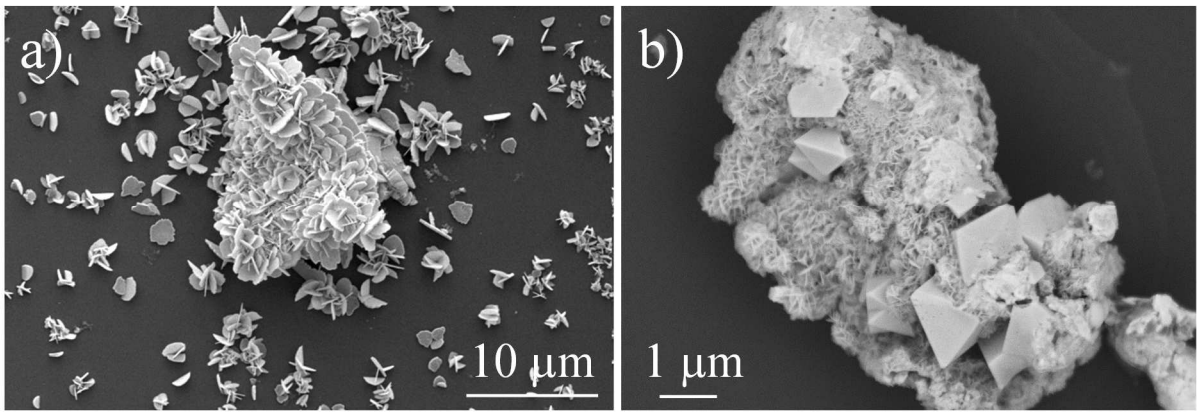

Supplemental material 1: a) Desert rose-like structure without and b) with octahedral.